

Electromagnetic Wave Scattering from Rough Boundaries Interfacing Inhomogeneous Media and Application to Snow-Covered Sea Ice

Alexander S. Komarov^{1, 2, *}, Lotfollah Shafai¹, and David G. Barber²

Abstract—In this study a new analytical formulation for electromagnetic wave scattering from rough boundaries interfacing inhomogeneous media is presented based on the first-order approximation of the small perturbation method. First, we considered a scattering problem for a single rough boundary embedded in a piecewise continuously layered medium. As a key step, we introduced auxiliary wave propagation problems that are aimed to link reflection and transmission coefficients in the layered media with particular solutions of one-dimensional wave equations at the mean level of the rough interface. This approach enabled us to express the final solution in a closed form avoiding a prior discretization of the inhomogeneous medium. Second, we naturally extended the obtained solution to an arbitrary number of rough interfaces separating continuously layered media. As a validation step, we demonstrated that available solutions in the literature represent special cases of our general solution. Furthermore, we showed that our numerical results agree well with published data. Finally, as a particular special case, we presented a formulation for scattering from inhomogeneous snow-covered sea ice when the dominant scattering occurs at the snow-ice and air-snow interfaces.

1. INTRODUCTION

Accelerated decline of the Arctic sea ice extent [1] and thickness [2, 3] causes dramatic changes in the coupled ocean-sea ice-atmosphere system. Over the past three decades the ice-albedo feedback mechanism played a major role in a pervasive increase in the amount of solar energy deposited in the upper Arctic Ocean, with maximum values of 4% per year [4]. Larger heat fluxes from the ocean to the atmosphere are expected to cause significant warming of the Arctic region [5]. Furthermore, extensive solar heating led to a sharp depletion of thick multiyear (MY) ice and concomitantly increased proportion of first-year (FY) ice. Monitoring, modeling and predicting these climatic changes in the Arctic is becoming increasingly important because of the increase in development of recently accessible Arctic resources.

Microwave radar remote sensing has been extensively used for detecting dynamic [6, 7] and thermodynamic changes [8] in sea ice. However, improved algorithms for extracting key parameters of sea ice from radar observations such as synthetic aperture radar (SAR) imagery are still required. To better understand the linkage between the geophysical and thermodynamic state of sea ice and radar signatures, modeling techniques for electromagnetic wave scattering from snow-covered sea ice are particularly important. These models should reproduce scattering characteristics in the bistatic case (when transmitter and receiver antennas are spanned in space) to anticipate future bistatic spaceborne SAR systems [9].

In the literature various approaches to modeling of electromagnetic wave scattering from rough surfaces can be found.

Received 12 November 2013, Accepted 31 December 2013, Scheduled 21 January 2014

* Corresponding author: Alexander S. Komarov (a_komarov@umanitoba.ca).

¹ Department of Electrical and Computer Engineering, University of Manitoba, Winnipeg, Manitoba, R3T 5V6, Canada. ² Centre for Earth Observation Science, University of Manitoba, Winnipeg, Manitoba, R3T 2N2, Canada.

Semi-empirical composite scattering models [10–12] allow to naturally account for volume scattering in sea ice (based on the radiative transfer theory [13]); however, the surface scattering terms in these models need to be separately determined from empirically or physically based theories.

All other models considered are based on solution of Maxwell’s equations. They can be classified into numerical and analytical (wave theory) methods. Unlike the radiative transfer models, the physical models are able to provide phase information as well.

Numerical finite-difference time-domain (FDTD) [14,15] and finite-volume time-domain (FVTD) [16] methods exactly solve Maxwell’s equations, within numerical approximation. These methods can account for surface and subsurface roughness and an arbitrary behavior of the dielectric constant within the media. However, the time domain methods require significant computational resources due to a number of reasons. Among them are (a) numerous realizations of the random rough surface, and (b) extremely fine mesh in the situations where absorption is high (e.g., sea water under the ice). Unfortunately, the computational constrains make the numerical methods difficult to apply to practical remote sensing problems such as simulation of temporal changes in SAR signatures over the sea ice.

Analytical methods are aimed to derive a closed-form solution of Maxwell’s equation under various approximations. These methods are not computationally expensive and thereby more suitable for practical geophysical applications. The small perturbation method (SPM) was introduced by Rice [17] in 1951 to analytically describe wave scattering from slightly rough surfaces. Since then the SPM theory was extended to solving more complex scattering problems. In [18] an SPM solution for wave scattering from a rough surface embedded in a three-layered structure was derived. Scattering from a layered structure with a rough upper boundary was treated in [19]. In [20] a unified formulation of perturbative solutions derived by [18,19] was presented. Later the SPM solution was extended to scattering from two [21] and several rough interfaces [22] embedded in a layered medium. The recent study by [22] presents an SPM solution for the medium treated as a number of homogeneous discrete layers separated by rough interfaces. Meanwhile, most natural media (e.g., snow, ice, soil) have continuous profiles of dielectric constants and a few rough interfaces separating the inhomogeneous media. Therefore, it is important to consider the SPM formalism for wave scattering from rough surfaces interfacing continuous dielectric fillings between them.

Our main goal is to build a geoscience user-oriented SPM solution expressed through physically meaningful reflection and transmission coefficients associated with the continuously layered media (e.g., snow, ice, soil). These reflection and transmission coefficients could be either modelled through discretization of the layered media, in some cases found analytically, or measured directly (in the field or laboratory).

An important application of the SPM theory is modeling of microwave scattering from the FY snow-covered sea ice. This type of ice is anticipated to prevail in the Arctic Ocean in the near future [23]. In the frequency range between 0.5 GHz (P-band) and 10 GHz (X-band) the dominant scattering mechanism for the FY ice is the surface scattering from two rough interfaces: air-snow and snow-ice interfaces [24]. Both interfaces are slightly rough in these frequency bands, and thereby, the SPM theory is applicable to model microwave interactions with snow-covered FY sea ice.

Thus, in this study we pursue three main objectives. (1) To derive a general analytical formulation for electromagnetic wave scattering from an arbitrary number of rough interfaces separating continuously layered media with the use of the first-order approximation of the SPM theory. The solution must be expressed through complex reflection and transmission coefficients associated with the inhomogeneous media. (2) To validate the obtained solution by treating special cases available in the literature and comparing numerical results with those available in the literature. (3) To present an analytical formulation for electromagnetic wave scattering from snow-covered sea ice as a special case of the general solution.

2. STATEMENT OF SCATTERING PROBLEM

Geometry of the general scattering problem is displayed in Figure 1 in cylindrical coordinates $\{\rho, z\}$. The area $z > 0$ is a free space with relative permittivity and permeability of one. Complex dielectric constant (CDC) and complex magnetic constant (CMC) of the inhomogeneous half space $z < 0$ are described by piecewise continuous functions through a set of continuous functions $\varepsilon_n(z)$, $\mu_n(z)$ such

that their derivatives are continuous within layers $-d_n < z < -d_{n-1}$. The continuously inhomogeneous media are separated by N rough interfaces located at $z = -d_n$, where $n = 0, 1, 2, \dots, N-1$, and $d_0 = 0$. Suppose, that roughness of interfaces is described by stationary random functions $\zeta_n(\boldsymbol{\rho})$ with zero average value $\langle \zeta_n(\boldsymbol{\rho}) \rangle = 0$, where the sharp brackets $\langle \dots \rangle$ denote ensemble averaging. A plane electromagnetic monochromatic wave with circular frequency ω , harmonic time dependence $e^{-i\omega t}$ and an arbitrary polarization is incident upon this structure. The incidence angle is $0 \leq \Theta_0 < \frac{\pi}{2}$ relative to the vertical axis z .

Our purpose is to determine electromagnetic fields in far zone in the upper half-space and to calculate the normalized radar cross-sections (NRCS) σ_{VV} , σ_{HH} , σ_{HV} and σ_{VH} as functions of azimuth and elevation angles in the upper half-space $z > 0$. We assume that the formulated problem is considered within the validity range of the first-order approximation of the SPM theory.

3. DERIVATION OF SOLUTION

First, we derive a formulation for a key scattering problem with a single rough interface $\zeta_n(\boldsymbol{\rho})$ located at $z = -d_n$, where $n = 0, 1, 2, \dots, N-1$, and $d_0 = 0$. Then we generalize the obtained solution for an arbitrary number of rough boundaries. The SPM formalism applies to surfaces with a small surface height variation and small surface slopes with respect to the incident wavelength [25]:

$$kL_n < 3, \quad k\sigma_n < 0.3, \quad \frac{\sigma_n}{L_n} < 0.3, \quad (1)$$

where k is the wave number in the medium, L_n the correlation length, and $\sigma_n = \sqrt{\langle \zeta_n^2 \rangle}$ the standard deviation of the rough surface $\zeta_n(\boldsymbol{\rho})$. Also, we assume that the gradient of the dielectric constant in the vicinity of the rough interface is small, i.e., $\left| \frac{\varepsilon'(-d_n \pm 0)}{\varepsilon(-d_n \pm 0)} \right| \sigma_n \ll 1$. Following the first-order approximation of the SPM formalism the electric and magnetic fields are expanded in a perturbation series [26–28] as follows:

$$\begin{aligned} \mathbf{E}(\boldsymbol{\rho}, z) &\approx \mathbf{E}^{(0)}(\boldsymbol{\rho}, z) + \mathbf{E}^{(1)}(\boldsymbol{\rho}, z) \\ \mathbf{H}(\boldsymbol{\rho}, z) &\approx \mathbf{H}^{(0)}(\boldsymbol{\rho}, z) + \mathbf{H}^{(1)}(\boldsymbol{\rho}, z) \end{aligned} \quad (2)$$

where $\mathbf{E}^{(0)}$, $\mathbf{H}^{(0)}$ are zero-order fields when the roughness is absent, and $\mathbf{E}^{(1)}$, $\mathbf{H}^{(1)}$ are first-order fields dependent on the roughness function [28]. The first-order fields represent a random component of the electromagnetic field due to the rough interface. Thus, the roughness influence is taken into account by a random additive component (first-order fields). To solve the scattering problem with only one rough interface at $z = -d_n$ zero-order and first-order fields must be defined in three regions: $z \geq 0$, $-d_n \leq z \leq 0$ and $z \leq -d_n$. Since we have the only rough interface at $z = -d_n$ we introduce the boundary conditions for zero-order and first-order fields at $z = 0$ and $z = -d_n$ as follows.

Zero-order approximation:

At $z = 0$:

$$\begin{aligned} \mathbf{E}_t^{(0)}(\boldsymbol{\rho}, +0) - \mathbf{E}_t^{(0)}(\boldsymbol{\rho}, -0) &= 0, \\ \mathbf{H}_t^{(0)}(\boldsymbol{\rho}, +0) - \mathbf{H}_t^{(0)}(\boldsymbol{\rho}, -0) &= 0. \end{aligned} \quad (3)$$

At $z = -d_n$:

$$\begin{aligned} \mathbf{E}_t^{(0)}(\boldsymbol{\rho}, -d_n + 0) - \mathbf{E}_t^{(0)}(\boldsymbol{\rho}, -d_n - 0) &= 0, \\ \mathbf{H}_t^{(0)}(\boldsymbol{\rho}, -d_n + 0) - \mathbf{H}_t^{(0)}(\boldsymbol{\rho}, -d_n - 0) &= 0. \end{aligned} \quad (4)$$

First-order approximation:

At $z = 0$:

$$\begin{aligned} \mathbf{E}_t^{(1)}(\boldsymbol{\rho}, +0) - \mathbf{E}_t^{(1)}(\boldsymbol{\rho}, -0) &= 0, \\ \mathbf{H}_t^{(1)}(\boldsymbol{\rho}, +0) - \mathbf{H}_t^{(1)}(\boldsymbol{\rho}, -0) &= 0. \end{aligned} \quad (5)$$

At the rough interface $z = -d_n$ [28]:

$$\begin{aligned}
\mathbf{E}_t^{(1)}(\boldsymbol{\rho}, -d_n + 0) - \mathbf{E}_t^{(1)}(\boldsymbol{\rho}, -d_n - 0) &= -\zeta_n(\boldsymbol{\rho}) \left[\left(\frac{\partial \mathbf{E}_t^{(0)}}{\partial z} \right)_{z=-d_n+0} - \left(\frac{\partial \mathbf{E}_t^{(0)}}{\partial z} \right)_{z=-d_n-0} \right] \\
&\quad - \nabla_{\perp} \zeta_n(\boldsymbol{\rho}) \left[E_z^{(0)}(\boldsymbol{\rho}, -d_n + 0) - E_z^{(0)}(\boldsymbol{\rho}, -d_n - 0) \right], \\
\mathbf{H}_t^{(1)}(\boldsymbol{\rho}, -d_n + 0) - \mathbf{H}_t^{(1)}(\boldsymbol{\rho}, -d_n - 0) &= -\zeta_n(\boldsymbol{\rho}) \left[\left(\frac{\partial \mathbf{H}_t^{(0)}}{\partial z} \right)_{z=-d_n+0} - \left(\frac{\partial \mathbf{H}_t^{(0)}}{\partial z} \right)_{z=-d_n-0} \right] \\
&\quad - \nabla_{\perp} \zeta_n(\boldsymbol{\rho}) \left[H_z^{(0)}(\boldsymbol{\rho}, -d_n + 0) - H_z^{(0)}(\boldsymbol{\rho}, -d_n - 0) \right],
\end{aligned} \tag{6}$$

where ∇_{\perp} is the gradient operator in the horizontal plane (x - y). Two sets of boundary conditions (3) (at $z = 0$) and (4) (at $z = -d_n$) are introduced in order to express zero-order fields through reflection and transmission coefficients associated with the inhomogeneous slab $-d_n \leq z \leq 0$ and the reflection coefficient from the half-space $z \leq -d_n$. Zero-order fields are required only to determine magnitudes of the first-order fields through boundary conditions (6).

Below we present formulations for zero-order and first-order fields.

3.1. Zero-order Fields

The total zero-order fields do not contain scattering components, and they should satisfy regular boundary conditions (3) and (4) at smooth interfaces.

Electromagnetic fields in an arbitrary layered medium are described by one-dimensional wave equations (for horizontal and vertical polarizations) with nonconstant coefficients dependent on the vertical coordinate z . These differential equations could potentially be solved numerically with respect to the electromagnetic fields. At the same time, the general solution for fields in a finite inhomogeneous layer can be expressed as a superposition of particular solutions of auxiliary Cauchy problems for a given wave equation. These solutions define the field distribution in the medium as well as magnitudes of reflected and transmitted waves at the interfaces.

3.1.1. Fields in the Air Half-space $z \geq 0$

In the upper half-space zero-order fields are presented as a superposition of the incident and specularly reflected plane waves. In our problem it is convenient to represent magnitudes of electric $\mathbf{E}^{(0)}$ and magnetic $\mathbf{H}^{(0)}$ fields through an expansion over the basis vectors $\{\hat{\rho}, \hat{\phi}, \hat{z}\}$ of the cylindrical coordinate system as our medium is homogeneous with respect to the azimuth angle and inhomogeneous with respect to the vertical coordinate only. This means that all the reflection and transmission coefficients do not depend on the azimuth angle. Also, the total field is symmetric with respect to the azimuth incidence angle Φ_0 . The basis vectors $\{\hat{\rho}, \hat{\phi}, \hat{z}\}$ of the cylindrical coordinate system are linked with the Cartesian unit vectors $\{\hat{x}, \hat{y}\}$ as follows:

$$\begin{aligned}
\hat{\rho} &= \hat{x} \cos \Phi_0 + \hat{y} \sin \Phi_0 \\
\hat{\phi} &= -\hat{x} \sin \Phi_0 + \hat{y} \cos \Phi_0.
\end{aligned}$$

It is worthwhile to point out that we consider a general case $\Phi_0 \neq 0$ in order to take into account more complex problems. For example, for anisotropic rough surfaces it could be more convenient to choose the coordinate system associated with the principal direction of anisotropy (and not with the direction of wave propagation).

The zero-order fields in the upper half space can be expressed as follows:

$$\begin{aligned}
\mathbf{E}^{(0)}(\boldsymbol{\rho}, z) &= \left\{ E_H \left[e^{-iw_0(q_0)z} + \Re_H(q_0) e^{iw_0(q_0)z} \right] \hat{\phi} - E_V \frac{w_0(q_0)}{k_0} \left[e^{-iw_0(q_0)z} - \Re_V(q_0) e^{iw_0(q_0)z} \right] \hat{\rho} \right. \\
&\quad \left. - E_V \frac{q_0}{k_0} \left[e^{-iw_0(q_0)z} + \Re_V(q_0) e^{iw_0(q_0)z} \right] \hat{z} \right\} e^{i\mathbf{q}_0 \boldsymbol{\rho}},
\end{aligned} \tag{7a}$$

$$\mathbf{H}^{(0)}(\boldsymbol{\rho}, z) = \frac{1}{Z_0} \left\{ E_V \left[e^{-iw_0(q_0)z} + \Re_V(q_0)e^{iw_0(q_0)z} \right] \hat{\phi} + E_H \frac{w_0(q_0)}{k_0} \left[e^{-iw_0(q_0)z} - \Re_H(q_0)e^{iw_0(q_0)z} \right] \hat{\rho} + E_H \frac{q_0}{k_0} \left[e^{-iw_0(q_0)z} + \Re_H(q_0)e^{iw_0(q_0)z} \right] \hat{z} \right\} e^{i\mathbf{q}_0 \boldsymbol{\rho}}. \quad (7b)$$

In (7a) and (7b) E_H and E_V denote magnitudes of the electric field of the incident wave for horizontal and vertical polarizations respectively. $k_0 = \omega\sqrt{\varepsilon_0\mu_0}$, and $Z_0 = \sqrt{\mu_0/\varepsilon_0}$ are the wave number and impedance in free space respectively; $\boldsymbol{\rho} = x\hat{x} + y\hat{y} = \rho(\hat{x} \cos \varphi + \hat{y} \sin \varphi)$ is a position vector of an observation point in the horizontal plane, where φ is an azimuth angle of the observation point. Also $\mathbf{q}_0 = k_0 \sin \Theta_0 (\hat{x} \cos \Phi_0 + \hat{y} \sin \Phi_0) = k_0 \sin \Theta_0 \hat{\rho}$ is the longitudinal wave vector which is a projection of the wave vector in the air onto the horizontal plane. The transverse wave number is a projection of the incident wave vector onto the axis z which can be written as $w_0(q_0) = \sqrt{k_0^2 - q_0^2} = k_0 \cos \Theta_0$. $\Re_{H,V}(q_0)$ are reflection coefficients from the entire inhomogeneous structure $z \leq 0$ for horizontal and vertical polarization with respect to electric and magnetic fields respectively. Solution (7a) and (7b) satisfy Maxwell's equations, boundary conditions at $z = 0$ and the conditions at infinity.

3.1.2. Fields in the Inhomogeneous Medium $-d_n \leq z \leq 0$

In the inhomogeneous medium a closed-form analytical solution does not exist; however, the solution can be expressed through piecewise continuous functions $u_H^{(0)}(q_0, z)$ and $u_V^{(0)}(q_0, z)$ as follows:

$$\mathbf{E}^{(0)}(\boldsymbol{\rho}, z) = \left\{ u_H^{(0)}(q_0, z)\hat{\phi} + \frac{1}{ik_0\varepsilon(z)}u_V'^{(0)}(q_0, z)\hat{\rho} - \frac{q_0}{k_0\varepsilon(z)}u_V^{(0)}(q_0, z)\hat{z} \right\} e^{i\mathbf{q}_0 \boldsymbol{\rho}}, \quad (8a)$$

$$\mathbf{H}^{(0)}(\boldsymbol{\rho}, z) = \frac{1}{Z_0} \left\{ u_V^{(0)}(q_0, z)\hat{\phi} - \frac{1}{ik_0\mu(z)}u_H'^{(0)}(q_0, z)\hat{\rho} + \frac{q_0}{k_0\mu(z)}u_H^{(0)}(q_0, z)\hat{z} \right\} e^{i\mathbf{q}_0 \boldsymbol{\rho}}, \quad (8b)$$

where

$$u_{H,V}^{(0)}(q_0, z) = c_{1H,V}^{(0)}u_{1H,V}(q_0, z) + c_{2H,V}^{(0)}u_{2H,V}(q_0, z). \quad (9)$$

In Equations (8a) and (8b) the stroke denotes a derivative with respect to z . In (9) $u_{1H,V}(q_0, z)$ and $u_{2H,V}(q_0, z)$ are particular solutions of one-dimensional wave equations for continuously layered media given as follows:

$$\mu(z) \frac{d}{dz} \left[\frac{1}{\mu(z)} \frac{du_{1,2H}(q_0, z)}{dz} \right] + [k^2(z) - q_0^2] u_{1,2H}(q_0, z) = 0, \quad (10)$$

$$\varepsilon(z) \frac{d}{dz} \left[\frac{1}{\varepsilon(z)} \frac{du_{1,2V}(q_0, z)}{dz} \right] + [k^2(z) - q_0^2] u_{1,2V}(q_0, z) = 0, \quad (11)$$

where $k(z) = k_0\sqrt{\varepsilon(z)\mu(z)}$. We accept that the introduced particular solutions satisfy the following initial conditions at the upper boundary $z = 0$:

$$u_{1H}(q_0, 0) = 1, \quad u'_{1H}(q_0, 0) = 0, \quad u_{2H}(q_0, 0) = 0, \quad u'_{2H}(q_0, 0) = i\mu_1(0)w_0(q_0), \quad (12)$$

$$u_{1V}(q_0, 0) = 1, \quad u'_{1V}(q_0, 0) = 0, \quad u_{2V}(q_0, 0) = 0, \quad u'_{2V}(q_0, 0) = i\varepsilon_1(0)w_0(q_0). \quad (13)$$

Wronskians of these particular solutions at $z = -d_n$ are equal to:

$$\left. \begin{aligned} u_{1H}(q_0, -d_n)u'_{2H}(q_0, -d_n) - u'_{1H}(q_0, -d_n)u_{2H}(q_0, -d_n) &= i\mu_n(-d_n)w_0(q_0) \\ u_{1V}(q_0, -d_n)u'_{2V}(q_0, -d_n) - u'_{1V}(q_0, -d_n)u_{2V}(q_0, -d_n) &= i\varepsilon_n(-d_n)w_0(q_0) \end{aligned} \right\}. \quad (14)$$

3.1.3. Fields in Half-space $z \leq -d_n$

In the lower half-space zero-order fields are given by:

$$\mathbf{E}^{(0)}(\boldsymbol{\rho}, z) = \left\{ v_H^{(0)}(q_0, z)\hat{\phi} + \frac{1}{ik_0\varepsilon(z)}v_V'^{(0)}(z)\hat{\rho} - \frac{q_0}{k_0\varepsilon(z)}v_V^{(0)}(q_0, z)\hat{z} \right\} e^{i\mathbf{q}_0 \boldsymbol{\rho}}, \quad (15a)$$

$$\mathbf{H}^{(0)}(\boldsymbol{\rho}, z) = \frac{1}{Z_0} \left\{ v_V^{(0)}(q_0, z) \hat{\phi} - \frac{1}{ik_0 \mu(z)} v_H^{(0)}(z) \hat{\rho} + \frac{q_0}{k_0 \mu(z)} v_H^{(0)}(q_0, z) \hat{z} \right\} e^{i\mathbf{q}_0 \boldsymbol{\rho}}, \quad (15b)$$

where $v_{H,V}^{(0)}(q_0, z)$ are solutions of wave Equations (10) and (11).

Plugging zero-order fields in boundary conditions (3) and (4) we obtain the following:

$$\begin{aligned} c_{1H,V}^{(0)} &= \frac{E_{H,V}}{iw_0(q_0)} [ik_0 M_{H,V}^n(q_0) u_{2H,V}(q_0, -d_n) + L_{H,V}^n(q_0) u'_{2H,V}(q_0, -d_n)], \\ c_{2H,V}^{(0)} &= -\frac{E_{H,V}}{iw_0(q_0)} [ik_0 M_{H,V}^n(q_0) u_{1H,V}(q_0, -d_n) + L_{H,V}^n(q_0) u'_{1H,V}(q_0, -d_n)], \end{aligned} \quad (16)$$

where

$$L_{H,V}^n(q_0) = \frac{w_0(q_0)}{w_n(q_0)} \frac{T_{H,V}^n(q_0)}{1 - r_{H,V}^n(q_0) R_{H,V}^n(q_0)} [1 + r_{H,V}^n(q_0)], \quad (17)$$

$$M_{H,V}^n(q_0) = \frac{w_0(q_0)}{k_0} \frac{T_{H,V}^n(q_0)}{1 - r_{H,V}^n(q_0) R_{H,V}^n(q_0)} [1 - r_{H,V}^n(q_0)]. \quad (18)$$

To obtain (16) we also needed to derive the following relationships:

$$\frac{v_H^{(0)}(q_0, -d_n)}{v_H^{(0)}(q_0, -d_n)} = -iw_n(q_0) \frac{\mu_{n+1}(-d_n)}{\mu_n(-d_n)} \frac{1 - r_H^n(q_0)}{1 + r_H^n(q_0)}, \quad (19a)$$

$$\frac{v_V^{(0)}(q_0, -d_n)}{v_V^{(0)}(q_0, -d_n)} = -iw_n(q_0) \frac{\varepsilon_{n+1}(-d_n)}{\varepsilon_n(-d_n)} \frac{1 - r_V^n(q_0)}{1 + r_V^n(q_0)}. \quad (19b)$$

In (17) and (18), $T_{H,V}^n(q_0)$ and $R_{H,V}^n(q_0)$ are transmission and reflection coefficients for a set of upper layers in the area $z > -d_n$, when the wave propagates from a homogeneous half-space $z < -d_n$ with CDC $\varepsilon_n(-d_n)$ and CMC $\mu_n(-d_n)$ for horizontal and vertical polarizations respectively.

In (17)–(19), $w_n(q_0) = \sqrt{k_0^2 \varepsilon_n(-d_n) \mu_n(-d_n) - q_0^2}$, $\text{Im} w_n \geq 0$; $r_{H,V}^n(q_0)$ are reflection coefficients in the problem where a plane wave is incident from a homogeneous area $z > -d_n$ with CDC $\varepsilon_n(-d_n)$ and CMC $\mu_n(-d_n)$ upon the inhomogeneous half-space $z < -d_n$.

If the rough boundary is located on top of the inhomogeneous structure (i.e., $n = 0$) then $T_{H,V}^0(q_0) = 1$, $R_{H,V}^0(q_0) = 0$, $r_{H,V}^0(q_0) = \Re_{H,V}(q_0)$. In this special case Equations (17) and (18) can be reduced as follows:

$$L_{H,V}^0(q_0) = 1 + \Re_{H,V}(q_0), \quad (20)$$

$$M_{H,V}^0(q_0) = \frac{w_0(q_0)}{k_0} [1 - \Re_{H,V}(q_0)]. \quad (21)$$

Using expressions (16) for coefficients $c_{1,2H,V}^{(0)}$ and Wronskians (14) in conjunction with equations for zero-order fields, the required expressions for boundary conditions (6) can be written as follows:

$$\begin{aligned} E_z^{(0)}(-d_n + 0) - E_z^{(0)}(-d_n - 0) &= -\frac{\Delta \varepsilon_{n+1} q_0}{\varepsilon_{n+1}(-d_n) k_0} E_V L_V^n(q_0) e^{i\mathbf{q}_0 \boldsymbol{\rho}}, \\ \frac{\partial \mathbf{E}_t^{(0)}}{\partial z} \Big|_{z=-d_n+0} - \frac{\partial \mathbf{E}_t^{(0)}}{\partial z} \Big|_{z=-d_n-0} &= -ik_0 \left[E_V \left(\Delta \mu_{n+1} \varepsilon_n(-d_n) + \frac{\Delta \varepsilon_{n+1} q_0^2}{\varepsilon_{n+1}(-d_n) k_0^2} \right) L_V^n(q_0) \hat{\rho}, \right. \\ &\quad \left. - \Delta \mu_{n+1} E_H M_H^n(q_0) \hat{\phi} \right] e^{i\mathbf{q}_0 \boldsymbol{\rho}} \end{aligned} \quad (22)$$

$$\begin{aligned} H_z^{(0)}(-d_n + 0) - H_z^{(0)}(-d_n - 0) &= \frac{1}{Z_0} \frac{\Delta \mu_{n+1} q_0}{\mu_{n+1}(-d_n) k_0} E_H L_H^n(q_0) e^{i\mathbf{q}_0 \boldsymbol{\rho}}, \\ \frac{\partial \mathbf{H}_t^{(0)}}{\partial z} \Big|_{z=-d_n+0} - \frac{\partial \mathbf{H}_t^{(0)}}{\partial z} \Big|_{z=-d_n-0} &= \frac{ik_0}{Z_0} \left[E_H \left(\Delta \varepsilon_{n+1} \mu_n(-d_n) + \frac{\Delta \mu_{n+1} q_0^2}{\mu_{n+1}(-d_n) k_0^2} \right) L_H^n(q_0) \hat{\rho} \right. \\ &\quad \left. + \Delta \varepsilon_{n+1} E_V M_V^n(q_0) \hat{\phi} \right] e^{i\mathbf{q}_0 \boldsymbol{\rho}}. \end{aligned} \quad (23)$$

In these expressions we introduced dielectric and magnetic contrasts at the boundary $z = -d_n$ as $\Delta\varepsilon_{n+1} = \varepsilon_{n+1}(-d_n) - \varepsilon_n(-d_n)$ and $\Delta\mu_{n+1} = \mu_{n+1}(-d_n) - \mu_n(-d_n)$ respectively.

3.2. First-order Fields in Integral Form

First-order approximation defines scattered fields by a rough surface. The scattered field is random and can be treated as a superposition of infinite number of plane waves outgoing in different directions from the rough interface. Therefore, it is convenient to represent the first-order fields through the Fourier integral. A Fourier transform of the rough surface is introduced as follows:

$$\tilde{\zeta}_n(\boldsymbol{\xi} - \mathbf{q}_0) = \iint \zeta_n(\boldsymbol{\rho}') e^{-i(\boldsymbol{\xi} - \mathbf{q}_0)\boldsymbol{\rho}'} d\boldsymbol{\rho}'. \quad (24)$$

The magnitudes of spectral functions can be found through boundary conditions for the first-order approximation. Below we provide integral representations of the first-order fields in three media.

3.2.1. Fields in the Air Half-Space $z \geq 0$

In the upper half-space the first-order fields from the n th rough boundary can be written as follows:

$$\mathbf{E}^{(1)}(\boldsymbol{\rho}, z) = \frac{1}{(2\pi)^2} \iint \left\{ a_H^{(1)n}(\boldsymbol{\xi}) \hat{\psi} + \frac{w_0(\boldsymbol{\xi})}{k_0} a_V^{(1)n}(\boldsymbol{\xi}) \hat{\xi} - \frac{\xi}{k_0} a_V^{(1)n}(\boldsymbol{\xi}) \hat{z} \right\} \tilde{\zeta}_n(\boldsymbol{\xi} - \mathbf{q}_0) e^{iw_0(\boldsymbol{\xi})z + i\boldsymbol{\xi}\boldsymbol{\rho}} d\boldsymbol{\xi}, \quad (25a)$$

$$\mathbf{H}^{(1)}(\boldsymbol{\rho}, z) = \frac{1}{Z_0(2\pi)^2} \iint \left\{ a_V^{(1)n}(\boldsymbol{\xi}) \hat{\psi} - \frac{w_0(\boldsymbol{\xi})}{k_0} a_H^{(1)n}(\boldsymbol{\xi}) \hat{\xi} + \frac{\xi}{k_0} a_H^{(1)n}(\boldsymbol{\xi}) \hat{z} \right\} \tilde{\zeta}_n(\boldsymbol{\xi} - \mathbf{q}_0) e^{iw_0(\boldsymbol{\xi})z + i\boldsymbol{\xi}\boldsymbol{\rho}} d\boldsymbol{\xi}, \quad (25b)$$

where $a_{H,V}^{(1)n}(\boldsymbol{\xi})$ are magnitudes of the scattered field. The functions under the integral sign are represented as expansions over a basis in the cylindrical coordinate system $\{\xi, \psi, z\}$ in the wave numbers' space. $\hat{\psi}$ and $\hat{\xi}$ are the azimuth and radial unit vectors associated with the floating coordinate system in the wave numbers' space. In (25) $d\boldsymbol{\xi} = \xi d\xi d\psi$ and the vertical component of the wave number of partial plane waves in free space is given by $w_0(\boldsymbol{\xi}) = \sqrt{k_0^2 - \xi^2}$, $\text{Im}w_0(\boldsymbol{\xi}) \geq 0$.

3.2.2. Fields in the Medium $-d_n \leq z \leq 0$

In the inhomogeneous medium the first-order fields can be given by:

$$\mathbf{E}^{(1)}(\boldsymbol{\rho}, z) = \frac{1}{(2\pi)^2} \iint \left\{ u_H^{(1)}(\boldsymbol{\xi}, z) \hat{\psi} + \frac{1}{ik_0\varepsilon(z)} u_V^{(1)}(\boldsymbol{\xi}, z) \hat{\xi} - \frac{\xi}{k_0\varepsilon(z)} u_V^{(1)}(\boldsymbol{\xi}, z) \hat{z} \right\} \tilde{\zeta}_n(\boldsymbol{\xi} - \mathbf{q}_0) e^{i\boldsymbol{\xi}\boldsymbol{\rho}} d\boldsymbol{\xi}, \quad (26a)$$

$$\mathbf{H}^{(1)}(\boldsymbol{\rho}, z) = \frac{1}{Z_0(2\pi)^2} \iint \left\{ u_V^{(1)}(\boldsymbol{\xi}, z) \hat{\psi} - \frac{1}{ik_0\mu(z)} u_H^{(1)}(\boldsymbol{\xi}, z) \hat{\xi} + \frac{\xi}{k_0\mu(z)} u_H^{(1)}(\boldsymbol{\xi}, z) \hat{z} \right\} \tilde{\zeta}_n(\boldsymbol{\xi} - \mathbf{q}_0) e^{i\boldsymbol{\xi}\boldsymbol{\rho}} d\boldsymbol{\xi}, \quad (26b)$$

where

$$u_{H,V}^{(1)}(\boldsymbol{\xi}, z) = c_{1H,V}^{(1)n}(\boldsymbol{\xi}) u_{1H,V}(\boldsymbol{\xi}, z) + c_{2H,V}^{(1)n}(\boldsymbol{\xi}) u_{2H,V}(\boldsymbol{\xi}, z). \quad (27)$$

In the last equation $u_{1,2H}(\boldsymbol{\xi}, z)$ and $u_{1,2V}(\boldsymbol{\xi}, z)$ are particular solutions of wave Equations (10) and (11) except that the longitudinal wave number q_0 is replaced by ξ .

We accept that the introduced particular solutions satisfy the following initial conditions at the upper boundary $z = 0$:

$$u_{1H}(\boldsymbol{\xi}, 0) = 1, \quad u'_{1H}(\boldsymbol{\xi}, 0) = 0, \quad u_{2H}(\boldsymbol{\xi}, 0) = 0, \quad u'_{2H}(\boldsymbol{\xi}, 0) = i\mu_1(0)w_0(\boldsymbol{\xi}), \quad (28)$$

$$u_{1V}(\boldsymbol{\xi}, 0) = 1, \quad u'_{1V}(\boldsymbol{\xi}, 0) = 0, \quad u_{2V}(\boldsymbol{\xi}, 0) = 0, \quad u'_{2V}(\boldsymbol{\xi}, 0) = i\varepsilon_1(0)w_0(\boldsymbol{\xi}). \quad (29)$$

3.2.3. Fields in the Half-Space $z \leq -d_n$

In the lower half-space the first-order fields can be represented as follows:

$$\mathbf{E}^{(1)}(\boldsymbol{\rho}, z) = \frac{1}{(2\pi)^2} \iint \left\{ v_H^{(1)}(\boldsymbol{\xi}, z) \hat{\psi} + \frac{1}{ik_0\varepsilon(z)} v_V^{(1)}(\boldsymbol{\xi}, z) \hat{\xi} - \frac{\xi}{k_0\varepsilon(z)} v_V^{(1)}(\boldsymbol{\xi}, z) \hat{z} \right\} \tilde{\zeta}_n(\boldsymbol{\xi} - \mathbf{q}_0) e^{i\boldsymbol{\xi}\boldsymbol{\rho}} d\boldsymbol{\xi}, \quad (30a)$$

$$\mathbf{H}^{(1)}(\boldsymbol{\rho}, z) = \frac{1}{Z_0(2\pi)^2} \iint \left\{ v_V^{(1)}(\boldsymbol{\xi}, z) \hat{\psi} - \frac{1}{ik_0\mu(z)} v_H'^{(1)}(\boldsymbol{\xi}, z) \hat{\xi} + \frac{\xi}{k_0\mu(z)} v_H^{(1)}(\boldsymbol{\xi}, z) \hat{z} \right\} \tilde{\zeta}_n(\boldsymbol{\xi} - \mathbf{q}_0) e^{i\boldsymbol{\xi}\boldsymbol{\rho}} d\boldsymbol{\xi}, \quad (30b)$$

where $v_{H,V}^{(1)}(\boldsymbol{\xi}, z)$ are solutions of wave Equations (10) and (11) with the replacement of q_0 by ξ .

3.3. Spectral Magnitudes of the Scattered Field from the Rough Surface

Substituting the first-order fields into the boundary conditions (5) at the smooth interface $z = 0$ and taking into account (28) and (29), we obtain the following:

$$c_{1H,V}^{(1)n}(\boldsymbol{\xi}) = c_{2H,V}^{(1)n}(\boldsymbol{\xi}) = a_{H,V}^{(1)n}(\boldsymbol{\xi}). \quad (31)$$

Then plugging the first-order fields in boundary conditions (6) accounting for Equations (22) and (23), and applying the Fourier transform to both sides of the obtained pair of equations we derive the following relationships for magnitudes $a_{H,V}^{(1)n}(\boldsymbol{\xi})$ in the air:

$$\begin{aligned} a_H^{(1)n}(\boldsymbol{\xi}) = & \frac{E_H \mu_n(-d_n) k_0^2}{2i w_0(\xi)} \left[-\Delta \varepsilon_{n+1} \mu_n(-d_n) L_H^n(q_0) L_H^n(\xi) \cos(\psi - \Phi_0) \right. \\ & \left. - \frac{\Delta \mu_{n+1} \xi q_0}{\mu_{n+1}(-d_n) k_0^2} L_H^n(q_0) L_H^n(\xi) + \frac{\Delta \mu_{n+1}}{\mu_n(-d_n)} M_H^n(q_0) M_H^n(\xi) \cos(\psi - \Phi_0) \right] \\ & - \frac{E_V \mu_n(-d_n) k_0^2}{2i w_0(\xi)} \left[\Delta \varepsilon_{n+1} M_V^n(q_0) L_H^n(\xi) - \frac{\Delta \mu_{n+1} \varepsilon_n(-d_n)}{\mu_n(-d_n)} L_V^n(q_0) M_H^n(\xi) \right] \sin(\psi - \Phi_0), \quad (32) \end{aligned}$$

$$\begin{aligned} a_V^{(1)n}(\boldsymbol{\xi}) = & -\frac{E_V \varepsilon_n(-d_n) k_0^2}{2i w_0(\xi)} \left[\Delta \mu_{n+1} \varepsilon_n(-d_n) L_V^n(q_0) L_V^n(\xi) \cos(\psi - \Phi_0) \right. \\ & \left. + \frac{\Delta \varepsilon_{n+1} \xi q_0}{\varepsilon_{n+1}(-d_n) k_0^2} L_V^n(q_0) L_V^n(\xi) - \frac{\Delta \varepsilon_{n+1}}{\varepsilon_n(-d_n)} M_V^n(q_0) M_V^n(\xi) \cos(\psi - \Phi_0) \right] \\ & + \frac{E_H \varepsilon_n(-d_n) k_0^2}{2i w_0(\xi)} \left[\Delta \mu_{n+1} M_H^n(q_0) L_V^n(\xi) - \frac{\Delta \varepsilon_{n+1} \mu_n(-d_n)}{\varepsilon_n(-d_n)} L_H^n(q_0) M_V^n(\xi) \right] \sin(\psi - \Phi_0). \quad (33) \end{aligned}$$

3.4. Normalized Radar Cross-Sections

First-order fields in far zone are estimated using the method of stationary phase [29]. Then, radar cross-sections are calculated through the Poynting vector of electromagnetic field in far zone. We omit details of this part and present the derived radar cross-sections for co- and cross-polarized components at the observation point (θ, φ) :

$$\sigma_{\alpha\beta}^n(\theta, \varphi) = \frac{k_0^4}{4\pi} \left| a_{\alpha\beta}^{(1)n}(\theta, \varphi) \right|^2 \tilde{K}_n(\mathbf{q} - \mathbf{q}_0), \quad (34)$$

where subscripts $\alpha = H, V$ and $\beta = H, V$ denote polarizations of the incident (α) and the scattered (β) waves respectively. In (34) we have:

$$a_{HH}^{(1)n}(\theta, \varphi) = \frac{2w_0(q)}{k_0^2 E_H} a_H^{(1)n}(\mathbf{q}) \Big|_{E_V=0}, \quad a_{VV}^{(1)n}(\theta, \varphi) = \frac{2w_0(q)}{k_0^2 E_V} a_V^{(1)n}(\mathbf{q}) \Big|_{E_H=0}, \quad (35)$$

$$a_{HV}^{(1)n}(\theta, \varphi) = \frac{2w_0(q)}{k_0^2 E_H} a_V^{(1)n}(\mathbf{q}) \Big|_{E_V=0}, \quad a_{VH}^{(1)n}(\theta, \varphi) = \frac{2w_0(q)}{k_0^2 E_V} a_H^{(1)n}(\mathbf{q}) \Big|_{E_H=0}. \quad (36)$$

Also $\mathbf{q} = k_0 \sin \theta (\hat{x} \cos \varphi + \hat{y} \sin \varphi)$; $\tilde{K}_n(\mathbf{q} - \mathbf{q}_0)$ is the spatial power spectral density of the roughness linked with the autocorrelation function $K_n(\boldsymbol{\rho}) = \langle \zeta_n(\boldsymbol{\rho} + \boldsymbol{\rho}') \zeta_n(\boldsymbol{\rho}') \rangle$ at interface $z = -d_n$ as follows:

$$\tilde{K}_n(\mathbf{q} - \mathbf{q}_0) = \iint K_n(\boldsymbol{\rho}) e^{-i(\mathbf{q} - \mathbf{q}_0)\boldsymbol{\rho}} d\boldsymbol{\rho}. \quad (37)$$

Magnitudes of the scattered field in the direction of observation (θ, φ) are the following:

$$a_{HH}^{(1)n}(\theta, \varphi) = i \left[\Delta \varepsilon_{n+1} \mu_n^2(-d_n) L_H^n(q_0) L_H^n(q) \cos(\varphi - \Phi_0) + \Delta \mu_{n+1} \frac{\mu_n(-d_n) q q_0}{\mu_{n+1}(-d_n) k_0^2} L_H^n(q_0) L_H^n(q) - \Delta \mu_{n+1} M_H^n(q_0) M_H^n(q) \cos(\varphi - \Phi_0) \right], \quad (38)$$

$$a_{VV}^{(1)n}(\theta, \varphi) = i \left[\Delta \mu_{n+1} \varepsilon_n^2(-d_n) L_V^n(q_0) L_V^n(q) \cos(\varphi - \Phi_0) + \Delta \varepsilon_{n+1} \frac{\varepsilon_n(-d_n) q q_0}{\varepsilon_{n+1}(-d_n) k_0^2} L_V^n(q_0) L_V^n(q) - \Delta \varepsilon_{n+1} M_V^n(q_0) M_V^n(q) \cos(\varphi - \Phi_0) \right], \quad (39)$$

$$a_{HV}^{(1)n}(\theta, \varphi) = -i [\Delta \mu_{n+1} \varepsilon_n(-d_n) M_H^n(q_0) L_V^n(q) - \Delta \varepsilon_{n+1} \mu_n(-d_n) L_H^n(q_0) M_V^n(q)] \sin(\varphi - \Phi_0), \quad (40)$$

$$a_{VH}^{(1)n}(\theta, \varphi) = i [\Delta \varepsilon_{n+1} \mu_n(-d_n) M_V^n(q_0) L_H^n(q) - \Delta \mu_{n+1} \varepsilon_n(-d_n) L_V^n(q_0) M_H^n(q)] \sin(\varphi - \Phi_0). \quad (41)$$

Thus, the general formulations for NRCS of the initial problem displayed in Figure 1 can be written as follows:

$$\sigma_{\alpha\beta}(\theta, \varphi) = \frac{k_0^4}{4\pi} \sum_{n=0}^{N-1} \left\{ \left| a_{\alpha\beta}^{(1)n}(\theta, \varphi) \right|^2 \tilde{K}_n(\mathbf{q} - \mathbf{q}_0) + \sum_{m \neq n} \text{Re} \left[a_{\alpha\beta}^{(1)m}(\theta, \varphi) a_{\alpha\beta}^{(1)n*}(\theta, \varphi) \right] \tilde{K}_{mn}(\mathbf{q} - \mathbf{q}_0) \right\}, \quad (42)$$

where the asterisk denotes the complex conjugate and the cross power spectral density between interfaces m and n is defined as follows:

$$\tilde{K}_{mn}(\mathbf{q} - \mathbf{q}_0) = \iint K_{mn}(\boldsymbol{\rho}) e^{-i(\mathbf{q} - \mathbf{q}_0) \cdot \boldsymbol{\rho}} d\boldsymbol{\rho}. \quad (43)$$

In the last equation the cross-correlation function between interfaces m and n

$$K_{mn}(\boldsymbol{\rho}) = \langle \zeta_m(\boldsymbol{\rho} + \boldsymbol{\rho}') \zeta_n(\boldsymbol{\rho}') \rangle.$$

If all rough surfaces are statistically independent, then the second term in Equation (42) disappears, and the total radar cross-section is a sum of radar cross-sections from each of the rough interfaces:

$$\sigma_{\alpha\beta}(\theta, \varphi) = \sum_{n=0}^{N-1} \sigma_{\alpha\beta}^n(\theta, \varphi). \quad (44)$$

It is worthwhile to note that for grazing elevation angles the accuracy of the SPM theory becomes lower. At grazing elevation angles the shadowing effects (which are negligible at other angles) start dominating [25]. These phenomena are not taken into account by the SPM theory. In the literature there are attempts to introduce additional factors accounting for the shadowing effects in the second-order approximation of the SPM theory for the cross-polarized signal [25]. In general, it is assumed that the SPM theory is valid within the range from 20 to 60 degrees of incidence and observation elevation angles. At the elevation angles close to nadir the mirror reflection appears. We would like to note that elevation angles of currently operational radar systems fall within the range of validity of the SPM theory. For example, incidence angles of Canadian RADARSAT-2 vary from 20 to 60 degrees [30].

3.5. Monostatic Scattering

In the monostatic case the receiver elevation and azimuth angles are $\theta = \Theta_0$ and $\varphi = \pi + \Phi_0$ respectively. Therefore, general equations from the previous section can be reduced to the following:

$$\sigma_{\alpha\alpha}^0 = \frac{k_0^4}{4\pi} \sum_{n=0}^{N-1} \left\{ \left| a_{\alpha\alpha}^{(1)n0} \right|^2 \tilde{K}_n(-2\mathbf{q}_0) + \sum_{m \neq n} \text{Re} \left[a_{\alpha\alpha}^{(1)m0} a_{\alpha\alpha}^{(1)n0*} \right] \tilde{K}_{mn}(-2\mathbf{q}_0) \right\}, \quad \alpha = H, V, \quad (45)$$

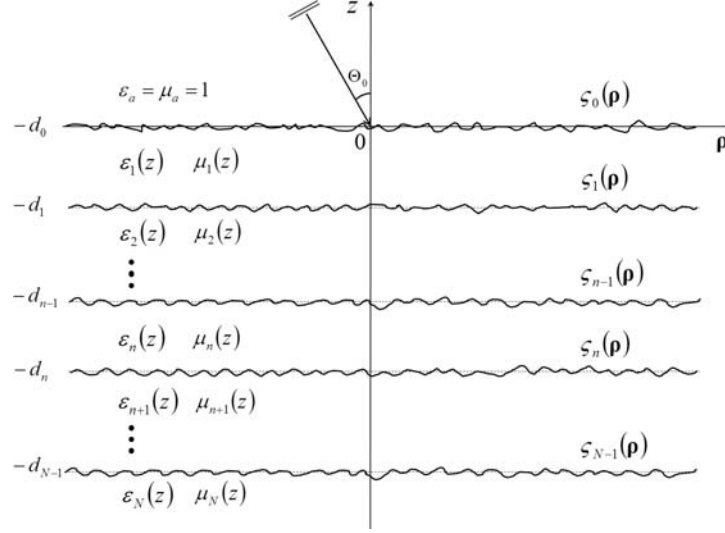


Figure 1. Illustration of a general problem for wave scattering from rough interfaces separating continuously layered media.

where

$$a_{HH}^{(1)n0} = i \left[\Delta\mu_{n+1} \frac{\mu_n(-d_n)q_0^2}{\mu_{n+1}(-d_n)k_0^2} [L_H^n(q_0)]^2 + \Delta\mu_{n+1} [M_H^n(q_0)]^2 - \Delta\varepsilon_{n+1}\mu_n^2(-d_n) [L_H^n(q_0)]^2 \right], \quad (46)$$

$$a_{VV}^{(1)n0} = i \left[\Delta\varepsilon_{n+1} \frac{\varepsilon_n(-d_n)q_0^2}{\varepsilon_{n+1}(-d_n)k_0^2} [L_V^n(q_0)]^2 + \Delta\varepsilon_{n+1} [M_V^n(q_0)]^2 - \Delta\mu_{n+1}\varepsilon_n^2(-d_n) [L_V^n(q_0)]^2 \right]. \quad (47)$$

The cross-polarization components of the first-order solution for the monostatic case are zeros. However, we expect that the second-order solution would provide a non-zero result for backscatter coefficients. The derivation of such a second-order solution for wave scattering from a homogeneous rough half-space is presented in [31]. Derivation of the second-order solution for wave scattering from rough boundaries interfacing inhomogeneous media is an important topic of future research.

4. VALIDATION OF SOLUTION

In this section we consider three special cases of the derived general solution. In all cases the permeability of all media is one. The obtained scattering characteristics for these cases are evaluated and compared with formulations available in the literature. Furthermore, we calculate bistatic scattering coefficients for a three-layered structure and compare the results with those available in the literature.

4.1. Scattering from a Rough Surface on Top of Homogeneous Half-Space

In the simplest case the wave is scattered by a rough surface $\zeta(\rho)$ on top of a homogeneous medium with CDC ε_1 . Then $L_{H,V}^0(q_0) = 1 + \Re_{H,V}^0(q_0)$, $M_{H,V}^0(q_0) = \cos \Theta_0 [1 - \Re_{H,V}^0(q_0)]$, where $\Re_{H,V}^0(q_0)$ are ordinary Fresnel reflection coefficients from a homogeneous half-space with CDC ε_1 [32]. It is not difficult to demonstrate that our general formulations for backscatter coefficients (45)–(47) are reduced to the following:

$$\sigma_{HH}^0 = \frac{4k_0^4}{\pi} \left| \frac{\varepsilon_1 - 1}{[\cos \Theta_0 + \sqrt{\varepsilon_1 - \sin^2 \Theta_0}]^2} \right|^2 \tilde{K}(-2\mathbf{q}_0) \cos^4 \Theta_0, \quad (48)$$

$$\sigma_{VV}^0 = \frac{4k_0^4}{\pi} \left| (\varepsilon_1 - 1) \frac{(\varepsilon_1 - 1) \sin^2 \Theta_0 + \varepsilon_1}{\left[\varepsilon_1 \cos \Theta_0 + \sqrt{\varepsilon_1 - \sin^2 \Theta_0} \right]^2} \right|^2 \tilde{K}(-2\mathbf{q}_0) \cos^4 \Theta_0, \quad (49)$$

where \tilde{K} is the spatial power spectral density of the rough surface. The obtained results are identical to those presented among other sources in [12, 25, 26].

4.2. Scattering from a Rough Surface Embedded in a Three-Layered Structure

Consider wave scattering from a rough interface embedded in a three layered medium displayed in Figure 2. The original solution of this problem was derived by Yarovoy et al. in [18], and an alternative formulation in terms of reflection and transmission coefficients was proposed in [20]. In this case each medium is homogeneous, i.e., $\varepsilon_1(z) = \varepsilon_1, -d_1 < z < 0, \varepsilon_2(z) = \varepsilon_2, -d_2 < z < -d_1, \varepsilon_3(z) = \varepsilon_3, z < -d_2$ and in Equations (17), (18) $n = 1$. Also it is possible to show that $T_H^1(q_0) = \frac{w_1(q_0)}{w_0(q_0)} \tau_{01H}(q_0) e^{iw_1(q_0)d_1}$, $T_V^1(q_0) = \frac{w_1(q_0)}{\varepsilon_1 w_0(q_0)} \tau_{01V}(q_0) e^{iw_1(q_0)d_1}$, and $R_{H,V}^1(q_0) = -r_{01H,V}(q_0) e^{2iw_1(q_0)d_1}$. Here $w_1(q_0) = k_0 \sqrt{\varepsilon_1 - \sin^2 \Theta_0}$, $\tau_{01H,V}(q_0)$ and $r_{01H,V}(q_0)$ are Fresnel transmission and reflection coefficients for the interface between air and medium 1 when wave is incident from the air. $r_{H,V}(q_0) \equiv r_{H,V}^1(q_0)$ are reflection coefficients from the two-layered structure (medium 2 and medium 3). Substituting Equations (17) and (18) taken for $n = 1$ into our general formulations for backscatter coefficients (45)–(47) we obtain:

$$\sigma_{HH}^0 = \frac{k_0^4}{4\pi} \left| (\varepsilon_2 - \varepsilon_1) \left(\frac{\tau_{01H}(q_0) e^{iw_1(q_0)d_1}}{1 + r_H(q_0) r_{01H}(q_0) e^{2iw_1(q_0)d_1}} \right)^2 [1 + r_H(q_0)]^2 \right|^2 \tilde{K}(-2\mathbf{q}_0), \quad (50)$$

$$\sigma_{VV}^0 = \frac{k_0^4}{4\pi} \left| \frac{\varepsilon_2 - \varepsilon_1}{\varepsilon_1} \left(\frac{\tau_{01V}(q_0) e^{iw_1(q_0)d_1}}{1 + r_V(q_0) r_{01V}(q_0) e^{2iw_1(q_0)d_1}} \right)^2 \left\{ \frac{\sin^2 \Theta_0}{\varepsilon_2} [1 + r_V(q_0)]^2 + \frac{\varepsilon_1 - \sin^2 \Theta_0}{\varepsilon_1} [1 - r_V(q_0)]^2 \right\} \right|^2 \tilde{K}(-2\mathbf{q}_0), \quad (51)$$

where \tilde{K} is the spatial power spectral density of the rough surface. These formulations are identical to those presented in [20] for Yarovoy model [18].

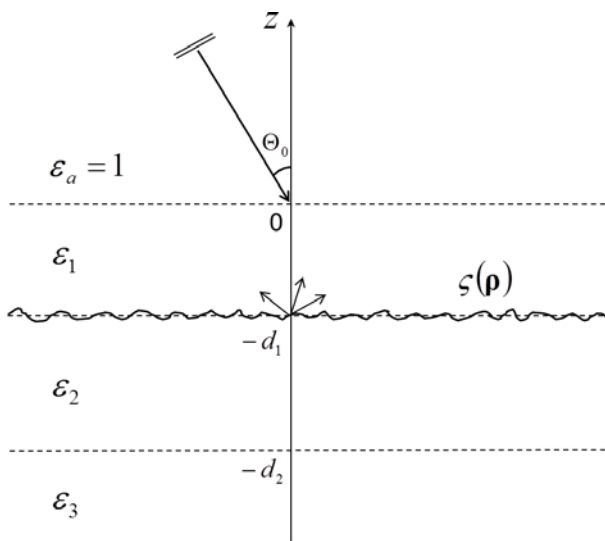


Figure 2. Geometry of scattering from a rough surface embedded in a three-layered medium.

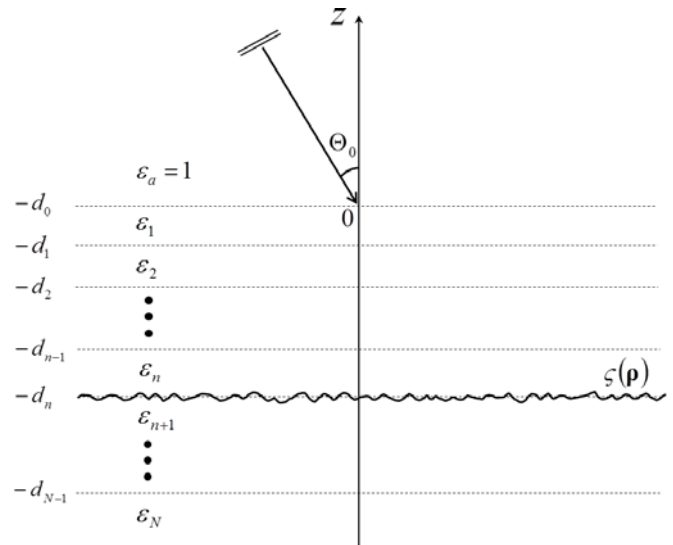


Figure 3. Geometry of scattering from a rough surface embedded in a layered medium.

4.3. Scattering from a Rough Surface Embedded in a Discretely Layered Medium

Consider a more general case when an electromagnetic wave is scattered by a rough surface embedded in a discretely layered medium shown in Figure 3.

Taking into account the phase change of the wave in layer n we obtain:

$$L_{H,V}^n(q) = \frac{w_0(q)}{w_n(q)} \frac{T_{H,V}^{n-1}(q)e^{iw_n(q)\Delta_n}}{1 - r_{H,V}^n(q)R_{H,V}^{n-1}(q)e^{2iw_n(q)\Delta_n}} [1 + r_{H,V}^n(q)], \quad (52)$$

$$M_{H,V}^n(q) = \frac{w_0(q)}{k_0} \frac{T_{H,V}^{n-1}(q)e^{iw_n(q)\Delta_n}}{1 - r_{H,V}^n(q)R_{H,V}^{n-1}(q)e^{2iw_n(q)\Delta_n}} [1 - r_{H,V}^n(q)], \quad (53)$$

where $\Delta_n = d_n - d_{n-1}$ is the layer thickness over the rough surface; $T_{H,V}^{n-1}(q)$ are transmission coefficients through the upper $(n-1)$ layers when the wave is incident from the half-space with CDC ε_n ; $R_{H,V}^{n-1}(q)$ are reflection coefficients from the upper $(n-1)$ layers when the wave is incident from the half-space with CDC ε_n ; $r_{H,V}^n(q)$ are reflection coefficients from the lower half-space when the wave is incident from the half-space with CDC ε_n .

Given (52) and (53), our general solution (38)–(42) can be reduced to the formulations presented by Imperatore et al. in [22]. At the same time, our solution is more general and elegant than the solution obtained by [22]. Unlike [22] we do not discretize the medium to derive the solution. Instead, we use properties of particular solutions of wave equations in the continuously layered media. Our solution is expressed through physically meaningful reflection and transmission coefficients for inhomogeneous media.

4.4. Numerical Results for a Three-Layered Structure

To further validate our model we calculate bistatic scattering coefficients for a special case illustrated in Figure 4. To compare the numerical results with the literature data we chose exactly the same scattering geometry and parameters of the media as considered in [22]. All the three rough interfaces have the same root mean square (RMS) height and correlation length. Each rough surface is described by the Gaussian autocorrelation function. The spectrum of this function is given as follows:

$$\tilde{K}_m(\mathbf{q} - \mathbf{q}_0) = \tilde{K}_m(|\mathbf{q} - \mathbf{q}_0|) = \pi L_m^2 \sigma_m^2 \exp\left(-\frac{L_m^2 |\mathbf{q} - \mathbf{q}_0|^2}{4}\right), \quad (54)$$

where σ_m , L_m are RMS height and correlation length of the rough interface $m = 0, 1, 2$.

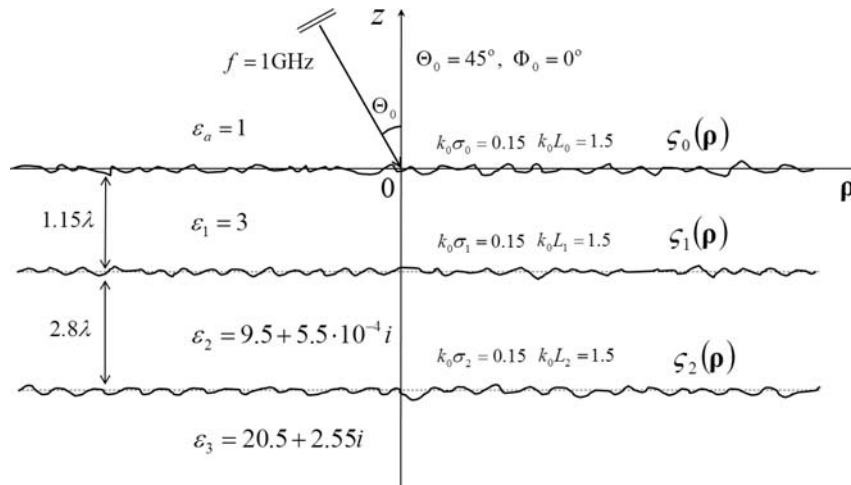


Figure 4. Three layered scattering geometry of the validation problem.

The incidence elevation and azimuth angles were chosen to be $\Theta_0 = 45^\circ$ and $\Phi_0 = 0^\circ$ respectively. The observation azimuth angle is $\varphi = 45^\circ$ while the observation elevation angle has been varied. Figure 5 demonstrates numerically calculated bistatic scattering coefficients for all polarizations (HH , VH , HV , and VV) from each rough boundary and from the whole structure (as a sum). In order to compare our

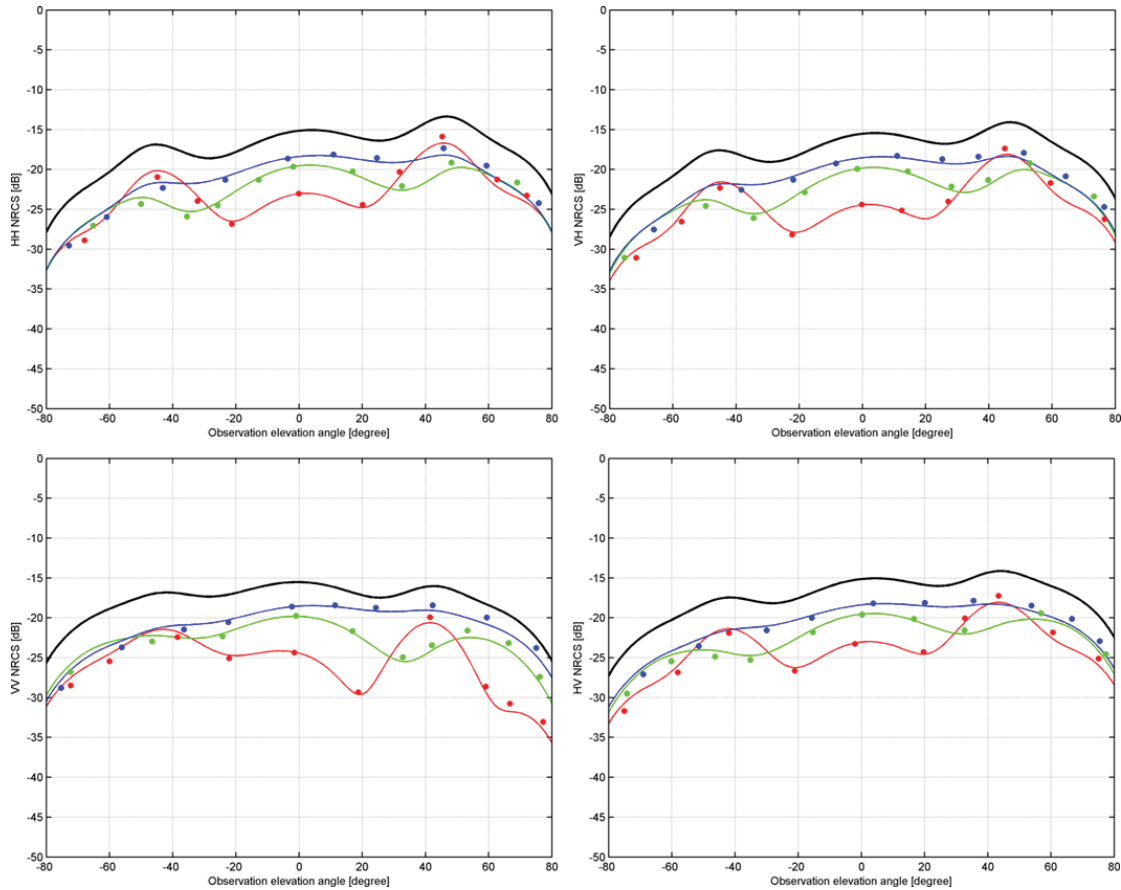


Figure 5. Comparison of numerical results computed according to our model (solid lines) against the (digitized) data presented in [22] (dots) for the geometry shown in Figure 4. Red: scattering from the upper boundary; green: scattering from the middle boundary; blue: scattering from the bottom boundary; black: total scattering.

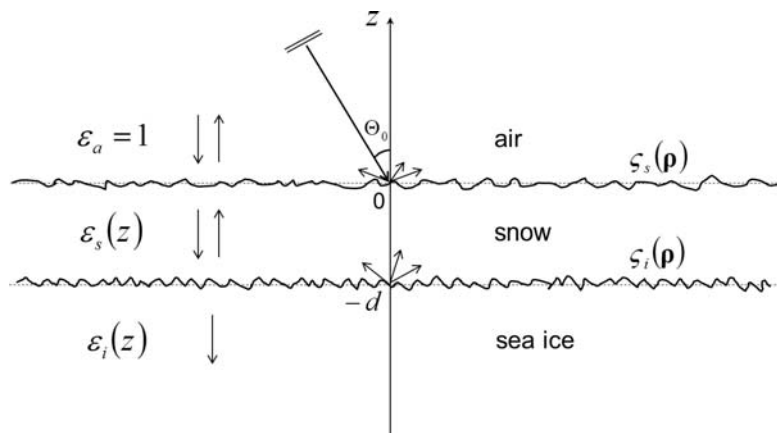


Figure 6. Illustration of wave scattering from snow-covered sea ice.

outputs with the results presented in literature we digitized 120 data points from Figure 4 of [22] and transferred them to our graphs. From Figure 5 one may observe a very good agreement between our numerical results and data from [22] for all polarizations. A small disparity can be attributed to the error coming from digitizing the low resolution graphs taken directly from the digital version of [22].

5. ELECTROMAGNETIC WAVE SCATTERING BY SNOW-COVERED SEA ICE

Electromagnetic wave scattering by snow-covered sea ice is an important special case of the general problem being considered. A plane electromagnetic wave is scattered by snow-covered sea ice. Snow and sea ice are characterized as continuous or discrete layered media. CDC of snow and sea ice are known functions $\varepsilon_s(z)$ and $\varepsilon_i(z)$ of vertical coordinate z as displayed in Figure 6. The roughness of the air-snow and snow-ice interfaces are described by stationary random functions $\zeta_s(\boldsymbol{\rho})$ and $\zeta_i(\boldsymbol{\rho})$ which define deviations from planes $z = 0$ and $z = -d$ respectively; d is the snow thickness. The dominant scattering mechanism in this problem is the surface scattering at the air-snow and snow-ice interfaces.

The obtained general solution (38)–(42) can be reduced to the snow-covered sea ice case by setting the number of rough interfaces to two and permeability of all media to one. Thus, the scattering component from rough sea ice can be written as follows:

$$\sigma_{HH}^{ice}(\theta, \varphi) = \frac{k_0^4 |\Delta\varepsilon_i|^2}{4\pi} |L_H(q_0)L_H(q)|^2 \cos^2(\varphi - \Phi_0) \tilde{K}_i(\mathbf{q} - \mathbf{q}_0), \quad (55)$$

$$\sigma_{VV}^{ice}(\theta, \varphi) = \frac{k_0^4 |\Delta\varepsilon_i|^2}{4\pi} \left| \frac{\varepsilon_s(-d)}{\varepsilon_i(-d)} \sin \Theta_0 \sin \theta L_V(q_0)L_V(q) - M_V(q_0)M_V(q) \cos(\varphi - \Phi_0) \right|^2 \tilde{K}_i(\mathbf{q} - \mathbf{q}_0), \quad (56)$$

$$\sigma_{HV}^{ice}(\theta, \varphi) = \frac{k_0^4 |\Delta\varepsilon_i|^2}{4\pi} |L_H(q_0)M_V(q)|^2 \sin^2(\varphi - \Phi_0) \tilde{K}_i(\mathbf{q} - \mathbf{q}_0), \quad (57)$$

$$\sigma_{VH}^{ice}(\theta, \varphi) = \frac{k_0^4 |\Delta\varepsilon_i|^2}{4\pi} |L_H(q)M_V(q_0)|^2 \sin^2(\varphi - \Phi_0) \tilde{K}_i(\mathbf{q} - \mathbf{q}_0), \quad (58)$$

where

$$L_{H,V}(q) = \frac{w_0(q)}{w_s(q)} \frac{T_{sH,V}(q)}{1 - r_{iH,V}(q)R_{sH,V}(q)} [1 + r_{iH,V}(q)], \quad (59)$$

$$M_{H,V}(q) = \frac{w_0(q)}{k_0} \frac{T_{sH,V}(q)}{1 - r_{iH,V}(q)R_{sH,V}(q)} [1 - r_{iH,V}(q)]. \quad (60)$$

In (55)–(58) $\Delta\varepsilon_i = \varepsilon_i(-d) - \varepsilon_s(-d)$ is the dielectric contrast between ice and snow at the rough interface. \tilde{K}_i is the spatial power spectral density of the ice-snow surface. In (59)–(60), $w_s(q) = \sqrt{k_0^2 \varepsilon_s(-d) - q^2}$, $w_0(q) = \sqrt{k_0^2 - q^2}$; $T_{sH,V}$ and $R_{sH,V}$ are transmission and reflection coefficients for the inhomogeneous snow layer when the wave is incident from the half-space with CDC $\varepsilon_s(-d)$; $r_{iH,V}$ are reflection coefficients from the inhomogeneous sea ice when the wave is incident from the half-space with CDC $\varepsilon_s(-d)$.

The scattering components from the rough snow can be written as follows:

$$\sigma_{HH}^{snow}(\theta, \varphi) = \frac{k_0^4 |\Delta\varepsilon_s|^2}{4\pi} |[1 + \Re_H(q_0)][1 + \Re_H(q)]|^2 \cos^2(\varphi - \Phi_0) \tilde{K}_s(\mathbf{q} - \mathbf{q}_0), \quad (61)$$

$$\begin{aligned} \sigma_{VV}^{snow}(\theta, \varphi) = & \frac{k_0^4 |\Delta\varepsilon_s|^2}{4\pi} \left| \frac{\sin \Theta_0 \sin \theta}{\varepsilon_s(0)} [1 + \Re_V(q_0)][1 + \Re_V(q)] \right. \\ & \left. - [1 - \Re_V(q_0)][1 - \Re_V(q)] \cos(\varphi - \Phi_0) \cos \Theta_0 \cos \theta \right|^2 \tilde{K}_s(\mathbf{q} - \mathbf{q}_0), \end{aligned} \quad (62)$$

$$\sigma_{HV}^{snow}(\theta, \varphi) = \frac{k_0^4 |\Delta\varepsilon_s|^2}{4\pi} |[1 + \Re_H(q_0)][1 - \Re_V(q)] \sin(\varphi - \Phi_0) \cos \theta|^2 \tilde{K}_s(\mathbf{q} - \mathbf{q}_0), \quad (63)$$

$$\sigma_{VH}^{snow}(\theta, \varphi) = \frac{k_0^4 |\Delta\varepsilon_s|^2}{4\pi} |[1 - \Re_V(q_0)][1 + \Re_H(q)] \sin(\varphi - \Phi_0) \cos \Theta_0|^2 \tilde{K}_s(\mathbf{q} - \mathbf{q}_0). \quad (64)$$

In (61)–(64) $\Delta\varepsilon_s = \varepsilon_s(0) - 1$ is the dielectric contrast at the air-snow interface; \tilde{K}_s is the spatial power spectral density of the snow surface; $\mathfrak{R}_{H,V}$ are reflection coefficients from the entire snow-covered sea ice structure at horizontal and vertical polarizations.

If the air-snow and snow-ice interfaces are statistically independent then the total NRCS is a sum of NRCS from the snow and sea ice:

$$\sigma_{\alpha\beta}(\theta, \varphi) = \sigma_{\alpha\beta}^{ice}(\theta, \varphi) + \sigma_{\alpha\beta}^{snow}(\theta, \varphi). \quad (65)$$

The last equation is a special case of the more general Equation (42) for two rough interfaces, i.e., $N = 2$. If the rough interfaces are correlated then according to (42) an additional correlation term should be introduced.

In the monostatic scattering case $\theta = \Theta_0$, $\varphi = \pi + \Phi_0$ and the cross-polarization component is zero. Therefore, the radar backscatter coefficients from sea ice can be presented as follows:

$$\sigma_{HH}^{0ice} = \frac{k_0^4 |\Delta\varepsilon_i|^2}{4\pi} |L_H(q_0)|^4 \tilde{K}_i(-2\mathbf{q}_0), \quad (66)$$

$$\sigma_{VV}^{0ice} = \frac{k_0^4 |\Delta\varepsilon_i|^2}{4\pi} \left| \frac{\varepsilon_s(-d)}{\varepsilon_i(-d)} \sin^2 \Theta_0 L_V^2(q_0) + M_V^2(q_0) \right|^2 \tilde{K}_i(-2\mathbf{q}_0), \quad (67)$$

$$\sigma_{HV}^{0ice} = \sigma_{VH}^{0ice} = 0. \quad (68)$$

The radar backscatter coefficients from the rough snow surface can be written as follows:

$$\sigma_{HH}^{0snow} = \frac{k_0^4 |\Delta\varepsilon_s|^2}{4\pi} |[1 + \mathfrak{R}_H(q_0)]|^4 \tilde{K}_s(-2\mathbf{q}_0), \quad (69)$$

$$\sigma_{VV}^{0snow} = \frac{k_0^4 |\Delta\varepsilon_s|^2}{4\pi} \left| \frac{\sin^2 \Theta_0}{\varepsilon_s(0)} [1 + \mathfrak{R}_V(q_0)]^2 + [1 - \mathfrak{R}_V(q_0)]^2 \cos^2 \Theta_0 \right|^2 \tilde{K}_s(-2\mathbf{q}_0), \quad (70)$$

$$\sigma_{HV}^{0snow} = \sigma_{VH}^{0snow} = 0. \quad (71)$$

The total radar backscatter from snow-covered sea ice is a sum of the backscatter coefficients from snow and sea ice similar to (65) (if the rough interfaces are statistically independent).

Modeling of dielectric properties of snow-covered sea ice (as a function of depth) is a separate problem which will be discussed in more details in our future publication on numerical modeling and measurements of scattering characteristics from real snow-covered sea ice. Here we briefly describe how the CDC of snow and sea ice can be found as functions of the vertical coordinate.

Snow on sea ice is a mixture of pure ice, air and brine (wicked from the sea ice surface). CDC of brine in snow is estimated as a function of temperature using Stogryn and Desargant model [33]. CDC of pure ice is nearly a constant (~ 3.15) in a wide range of frequencies [10]. The brine volume content in snow can be found through sea ice surface temperature and salinity (according to [34]) as well as snow density (which is a function of depth). We use physical properties of snow and sea ice from our field campaigns in the Arctic Ocean. There are a few dielectric models for estimating the CDC of moist snow (such as [35, 36]). However, a reliable dielectric mixture model for estimating the CDC of brine wetted snow on top of sea ice has not been developed. At the same time it has been shown that the refractive mixture model (which is linear with respect to refractive indices) is effective for sea ice [37]. In addition, the refractive mixture model has been proven to be the most accurate for wet soils [38]. Using this mixture model with input physical parameters measured in the field we obtain the CDC of snow as a function of depth.

The CDC of sea ice is calculated using the refractive mixture model for an isotropic two-phase medium consisting of pure ice and brine inclusions. In the study by [37] it was found that the refractive dielectric mixture model agrees very well with the dielectric measurements of sea ice reported in [39]. The brine volume of sea ice can be estimated as a function of ice temperature and bulk salinity according to [40]. The CDC of brine in sea ice can be found through the Debye relaxation model with temperature dependent parameters empirically derived by [33]. In the field campaigns we usually conduct measurements of temperature and bulk salinity as functions of sea ice depth (see e.g., [8]). Therefore, the CDC of sea ice is also derived as a function of depth.

We note that, if necessary, the sea water below the ice and the rough ice-water interface can be naturally included in the obtained formulation, but this is not the usual case as the penetration depth in natural FY sea ice is on the order of the wavelength (e.g., 5.5 cm in C-band and 21 cm in L-band) while FY ice grows to about 2 m thick by winters end. At the same time, if we model scattering characteristics from newly formed sea ice (with no snow cover) with the thickness around 10–20 cm, then the sea water half-space below the ice must be introduced. In this case the CDC of sea water can be found using the Debye-based model by Stogryn [41].

6. CONCLUSION

In this study we present a new analytical formulation for electromagnetic wave scattering from an arbitrary number of rough surfaces interfacing continuously layered media and derived a solution for wave scattering from snow-covered sea ice as a special case of the general problem. We solved Maxwell's equations within the first-order approximation of the SPM theory. First, we derived a solution for wave scattering from a single rough boundary while the other rough interfaces are absent. A key step in this solution is the introduction of two auxiliary problems on wave propagation in inhomogeneous media. In the first problem a plane wave is incident upon a piecewise continuously layered medium located above the rough interface from a medium with an arbitrary CDC and CMC. This problem allowed to link the reflection and transmission coefficients for the layered slab with the wave equations' particular solutions and their normal derivatives at the bottom of this slab. In the second problem a plane wave is incident upon a piecewise continuously layered medium located below the rough surface from the same medium as in the first problem. In this problem reflection coefficients from this medium are linked with the wave equations' particular solutions and their normal derivatives at the mean level of the rough interface. The results obtained in these two problems in conjunction with the boundary conditions allowed us to derive necessary equations for zero-order fields and their normal derivatives at the mean level of the rough interface. According to the SPM theory, these equations for zero-order fields are substituted into the boundary conditions for first-order fields. The first-order fields are represented through the Fourier integral over the partial plane waves outgoing from the rough surface. The under integral functions are written analogously to the first-order fields using particular solutions of the wave equations. Similarly to the zero-order case we found a link between the particular solutions of wave equations at the rough interface with reflection and transmission coefficients. Boundary conditions for the first-order fields enabled to resolve magnitudes of the scattered fields in the air. Finally, the radar characteristics are derived through the analytical evaluation of the Fourier integrals in far zone.

In our formulation we avoided any discretization of the continuously layered media; instead, we introduced particular solutions of wave equations and associated with them reflection and transmission coefficients at the rough interface. Such an approach makes our solution compact and physically meaningful. For example, the symmetry of the bi-static solution with respect to transmitting and receiving points is straightforward. The solution obtained for a single rough interface is naturally expanded to an arbitrary number of rough boundaries interfacing continuously layered media.

To validate the derived general solution we considered three special cases of the scattering problem. We demonstrated that our solution can be reduced to the formulations available in the literature including the most recent solution [22]. Furthermore we showed that our numerical results for wave scattering from a three-layered structure agree very well with those presented in [22].

We would like to point out that our formulation has been expressed through physically meaningful reflection and transmission coefficients associated with continuously layered media. To numerically implement the model, these coefficients must be estimated separately. For example, they can be computed using the following approaches: (1) invariant embedding method (where the inhomogeneous media are discretized) [42], (2) Runge Kutta method directly applied to one-dimensional wave equations (with non-constant coefficients), (3) analytical exact or analytical approximate approaches (applied in some cases) to solving the differential wave equations with non-constant coefficients. In practice, we use the invariant embedding approach [42].

The novelty of our model can be outlined as follows:

1. The obtained formulation is user-oriented and convenient for practical geophysical remote sensing applications. Our solution operates with physically meaningful reflection and transmission

coefficients associated with certain geophysical media (e.g., snow, ice, soil, etc.).

2. Our solution is fairly flexible because the numerical implementation can be split into two separate algorithmic units: (a) estimation of the reflection and transmission coefficients for inhomogeneous media using the approach that is best suited to a given structure of the inhomogeneous media; (b) calculation of scattering characteristics by plugging in these coefficients in the general solution.
3. If the complex reflection and transmission coefficients (for layered media) can be directly measured in the field (using, for example, a portable vector network analyzer), then the obtained values (at a given frequency) can be plugged in our model. In this case step (a) from the previous point is not required.
4. It appears that our analytical formulation is the only solution for wave scattering from layered media where both the complex dielectric and complex magnetic constants are continuous functions of depth.
5. Mathematical derivation and final formulation of our model is quite compact and at the same time general and physically meaningful compared to the previous solutions.

As the final step of this study, we presented an important special case of our formulation for wave scattering from snow-covered sea ice where both air-snow and snow-ice interfaces are rough and snow and ice are continuously layered media. The developed theory could be beneficial for the interpretation of sequential SAR signatures over snow-covered sea ice and inverse modeling. Beyond polar applications, the obtained theoretical formulation could be useful in remote sensing of various environmental media (e.g., snow-covered soil).

In our ongoing work we are currently validating this theory against in-situ C-band scatterometer measurements collected over natural snow-covered sea ice in the Canadian Arctic and experimentally grown sea ice at the Sea Ice Environmental Research Facility (SERF) at the University of Manitoba.

ACKNOWLEDGMENT

The work of A. S. Komarov was supported by a Canada Graduate Scholarship (CGS-D3) from the Natural Sciences and Engineering Research Council of Canada (NSERC); that of D. G. Barber was supported in part by the Canada Research Chairs (CRC) program and NSERC grants.

REFERENCES

1. Comiso, J., C. Parkinson, R. Gersten, and L. Stock, "Accelerated decline in the Arctic sea ice cover," *Geophys. Res. Lett.*, Vol. 35, L01703, Jan. 2008.
2. Kwok, R. and D. Rothrock, "Decline in Arctic sea ice thickness from submarine and ICESat records: 1958–2008," *Geophys. Res. Lett.*, Vol. 36, L15501, Aug. 2009.
3. Kwok, R. and N. Untersteiner, "The thinning of Arctic sea ice," *Physics Today*, Vol. 64, No. 4, 36–41, Apr. 2011.
4. Perovich, D. K., B. Light, H. Eicken, K. F. Jones, K. Runciman, and S. V. Nghiem, "Increasing solar heating of the Arctic Ocean and adjacent seas, 1979–2005: Attribution and role in the ice-albedo feedback," *Geophys. Res. Lett.*, Vol. 34, L19505, Oct. 2007, DOI:10.1029/2007GL031480.
5. Serreze, M. C., M. M. Holland, and J. Stroeve, "Perspectives on the Arctic's shrinking ice cover," *Science*, Vol. 315, 1533–1536, Mar. 2007, DOI:10.1126/science.1139426.
6. Komarov, A. S. and D. G. Barber, "Sea ice motion tracking from sequential dual-polarization RADARSAT-2 images," *IEEE Trans. Geosci. Remote Sens.*, Vol. 52, No. 1, 121–136, Jan. 2014.
7. Thomas, M., C. Kambhamettu, and C. Geiger, "Motion tracking of discontinuous sea ice," *IEEE Trans. Geosci. Remote Sens.*, Vol. 49, No. 12, 5064–5079, Dec. 2011.
8. Isleifson, D., B. Hwang, D. Barber, R. Scharien, and L. Shafai, "C-Band polarimetric backscattering signatures of newly formed sea ice during fall freeze-up," *IEEE Trans. on Geosci. Remote Sens.*, Vol. 48, No. 8, 3256–3267, Aug. 2010.

9. Moreira, A., P. Prats-Iraola, M. Younis, G. Kreiger, I. Hajnsek, and K. P. Papathanassiou, "A tutorial on synthetic aperture radar," *IEEE Geosci. and Rem. Sens. Magazine*, Vol. 1, No. 1, 6–43, Mar. 2013.
10. Ulaby, F. T., R. K. Moore, and A. K. Fung, *Microwave Remote Sensing: Active and Passive*, Vol. 3, Artech House, Norwood, MA, 1986.
11. Kim, Y. S., R. Onstott, and R. Moore, "Effect of a snow cover on microwave backscatter from sea ice," *IEEE J. Ocean. Eng.*, Vol. 9, No. 5, 383–388, Dec. 1984.
12. Carsey, F. D., *Microwave Remote Sensing of Sea Ice*, Geophysical Monograph 68, American Geophysical Union, 1992.
13. Ishimaru, A., *Wave Propagation and Scattering in Random Media*, Vol. 1–2, Academic, New York, 1978.
14. Hastings, F. D., J. B. Schneider, and S. L. Broschat, "A Monte-Carlo FDTD technique for rough surface scattering," *IEEE Trans. Antennas Propag.*, Vol. 43, No. 11, 1183–1191, Nov. 1995.
15. Nassar, E. M., J. T. Johnson, and R. Lee, "A numerical model for electromagnetic scattering from sea ice," *IEEE Trans. Geosci. Remote Sens.*, Vol. 38, No. 3, 1309–1319, May 2000.
16. Isleifson, D., I. Jeffrey, L. Shafai, J. LoVetri, and D. G. Barber, "A Monte Carlo method for simulating scattering from sea ice using FVTD," *IEEE Trans. Geosci. Remote Sens.*, Vol. 50, No. 7, 2658–2668, Jul. 2012.
17. Rice, S. O., "Reflection of electromagnetic waves from slightly rough surfaces," *Commun. Pure Appl. Math.*, Vol. 4, Nos. 2–3, 351–378, Aug. 1951, <http://dx.doi.org/10.1002/cpa.3160040206>.
18. Yarovoy, A. G., R. V. de Jongh, and L. P. Ligthard, "Scattering properties of a statistically rough interface inside a multilayered medium," *Radio Sci.*, Vol. 35, No. 2, 455–462, 2000.
19. Fuks, I. M., "Wave diffraction by a rough boundary of an arbitrary plane-layered medium," *IEEE Trans. Antennas Propag.*, Vol. 49, No. 4, 630–639, Apr. 2001.
20. Franceschetti, G., P. Imperatore, A. Iodice, D. Riccio, and G. Ruello, "Scattering from layered structures with one rough interface: A unified formulation of perturbative solutions," *IEEE Trans. Geosci. Remote Sens.*, Vol. 46, No. 6, 1634–1643, Jun. 2008.
21. Tabatabaenejad, A. and M. Moghaddam, "Bistatic scattering from dielectric structures with two rough boundaries using the small perturbation method," *IEEE Trans. Geosci. Remote Sens.*, Vol. 44, No. 8, Aug. 2006.
22. Imperatore, P., A. Iodice, and D. Riccio, "Electromagnetic wave scattering from layered structures with an arbitrary number of rough interfaces," *IEEE Trans. Geosci. Remote Sens.*, Vol. 47, No. 4, 1056–1072, Apr. 2009.
23. Barber, D. G., R. Galley, M. G. Asplin, R. De Abreu, K.-A. Warner, M. Pucko, M. Gupta, S. Prinsenber, and S. Julien, "Perennial pack ice in the southern Beaufort Sea was not as it appeared in the summer of 2009," *Geophys. Res. Lett.*, Vol. 36, L24501, Oct. 2009.
24. Barber, D. G., "Microwave remote sensing, sea ice and Arctic climate," *Phys. Can.*, Vol. 61, 105–111, Sep. 2005.
25. Fung, A. K. and K. S. Chen, *Microwave Scattering and Emission Models for Users*, Artech House, Boston, MA, 2010.
26. Ulaby, F. T., R. K. Moore, and A. K. Fung, *Microwave Remote Sensing: Active and Passive*, Vol. 2, Artech House, Norwood, MA, 1990.
27. Fung, A. K., *Microwave Scattering and Emission Models and Their Applications*, Artech House, Boston, MA, 1994.
28. Valenzuela, G. R., "Theories for the interactions of electromagnetic and oceanic waves: A review," *Boundary Layer Meteorol.*, Vol. 13, 61–85, 1978.
29. Collin, R. E., *Antennas and Radio Wave Propagation*, McGraw-Hill, New York, 1985.
30. *RADARSAT-2 Product Description RN-SP-52-1238*, MacDonald, Dettwiler and Associates Ltd., Richmond, BC, Canada, 2009.
31. Tsang, L. and J. A. Kong, *Scattering of Electromagnetic Waves: Advanced Topics*, Wiley Interscience, 2001.

32. Ulaby, F. T., R. K. Moore, and A. K. Fung, *Microwave Remote Sensing: Active and Passive*, Vol. 1, Artech House, Norwood, MA, 1986.
33. Stogryn, A. and G. D. Desargant, "The dielectric properties of brine in sea ice at microwave frequencies," *IEEE Trans. Antennas Propag.*, Vol. 33, No. 5, 523–532, May 1985.
34. Drinkwater, M. R. and G. B. Crocker, "Modeling changes in the dielectric and scattering properties of young snow covered sea ice at GHz frequencies," *J. Glaciology*, Vol. 34, No. 118, 274–282, 1988.
35. Hallikainen, M., F. Ulaby, and M. Abdelrazik, "Dielectric properties of snow in the 3 to 37 GHz range," *IEEE Trans. Antennas Propag.*, Vol. 34, No. 11, 1329–1340, Nov. 1986.
36. Khenchaf, A., "Bistatic reflection of electromagnetic waves from random rough surfaces. Application to the sea and snowy-covered surfaces," *Eur. Phys. J. Applied Physics*, Vol. 14, 45–62, 2001.
37. Gloersen, P. and J. K. Larabee, *An Optical Model for the Microwave Properties of Sea Ice*, NASA TM-83865, NASA Goddard Space Flight Center, Greenbelt, Maryland, 1981.
38. Mironov, V. L., M. C. Dobson, V. H. Kaupp, S. A. Komarov, and V. N. Kleshchenko, "Generalized refractive mixing dielectric model for moist soils," *IEEE Trans. Geosci. Remote Sens.*, Vol. 42, No. 4, 773–785, Apr. 2004.
39. Vant, M. R., R. B. Gray, R. O. Ramseier, and V. Makios, "Dielectric properties of fresh and sea ice at 10 and 35 GHz," *J. Appl. Phys.*, Vol. 45, No. 11, 4712–4717, 1974.
40. Frankenstein, G. and R. Garner, "Equations for determining the brine volume of sea ice from — 0.5 C to –22.9 C," *J. Glaciol.*, Vol. 6, No. 48, 943–944, 1967.
41. Stogryn, A., "Equations for calculating the dielectric constant of saline water," *IEEE Trans. Microwave Theory Thech.*, Vol. 19, 733–736, 1971.
42. Bellman, R. and R. Vasudevan, *Wave Propagation — An Invariant Embedding Approach*, D. Reidel Publishing Company, 1986.